nature cell biology

Microtubules induce self-organization of polarized PAR domains in *Caenorhabditis elegans* zygotes

Fumio Motegi[1], Seth Zonies[1], Yingsong Hao[1], Adrian A. Cuenca[1], Erik Griffin[1] and Geraldine Seydoux[1,2]

A hallmark of polarized cells is the segregation of the PAR polarity regulators into asymmetric domains at the cell cortex[1,2]. Antagonistic interactions involving two conserved kinases, atypical protein kinase C (aPKC) and PAR-1, have been implicated in polarity maintenance[1,2], but the mechanisms that initiate the formation of asymmetric PAR domains are not understood. Here, we describe one pathway used by the sperm-donated centrosome to polarize the PAR proteins in *Caenorhabditis elegans* zygotes. Before polarization, cortical aPKC excludes PAR-1 kinase and its binding partner PAR-2 by phosphorylation. During symmetry breaking, microtubules nucleated by the centrosome locally protect PAR-2 from phosphorylation by aPKC, allowing PAR-2 and PAR-1 to access the cortex nearest the centrosome. Cortical PAR-1 phosphorylates PAR-3, causing the PAR-3–aPKC complex to leave the cortex. Our findings illustrate how microtubules, independently of actin dynamics, stimulate the self-organization of PAR proteins by providing local protection against a global barrier imposed by aPKC.

Newly fertilized *C. elegans* zygotes have no predetermined anterior/posterior polarity. Before symmetry breaking, the PDZ domain proteins PAR-3 and PAR-6 and the kinase aPKC PKC-3 ('anterior PARs') are uniformly distributed at the cell cortex, and keep the kinase PAR-1 and the RING protein PAR-2 ('posterior PARs') in the cytoplasm. During symmetry breaking, the sperm centrosome (or microtubule-organizing centre, MTOC) contacts the cortex[1,2] eliciting two changes: actomyosin flows directed away from the MTOC (ref. 3), and recruitment of PAR-2 to the cortex nearest the MTOC (Fig. 1a; ref. 4). Actomyosin flows and PAR-2 function in parallel to displace anterior PARs from the cortex, allowing PAR-1 to also load on the posterior cortex. After cortical flows cease, PAR-2 becomes essential to prevent anterior PARs from returning to the posterior cortex (polarity maintenance)[3,5]. In this study, we investigate how the MTOC recruits PAR-2 to the cortex, and how PAR-2 in turn displaces anterior PARs.

We first examined PAR-2 dynamics in fixed zygotes depleted of the myosin regulatory light chain MLC-4 (ref. 6; Fig. 1 and Supplementary Fig. S1a). *mlc-4(RNAi)* zygotes do not develop cortical flows and depend solely on PAR-2 for symmetry breaking[4]. Before symmetry breaking, PAR-2 was in the cytoplasm and weakly enriched at the MTOC core (Fig. 1b and Supplementary Fig. S1a). During symmetry breaking, PAR-2 appeared on the cortex. In 21 of 28 (endogenous PAR-2) and 25 of 30 (GFP::PAR-2) zygotes fixed at this stage, PAR-2 was unevenly distributed on the cortex, with the highest levels at the microtubule-dense core of the MTOC (Fig. 1c and Supplementary Fig. S1a). The plasma membrane marker mCherry::PH^{PLC} was uniformly distributed at this stage (Supplementary Fig. S1a). After symmetry breaking, PAR-2 distribution on the cortex became more uniform (Fig. 1d) and the PAR-2 domain expanded to reach $32 \pm 5.2\%$ of the embryo's circumference (Fig. 1f). Live-cell imaging confirmed that the PAR-2 domain correlates with the site of MTOC–cortex contact (Supplementary Fig. S1c). Treatments that interfere with microtubule nucleation yielded zygotes that formed no cortical GFP::PAR-2 domains, or domains that were significantly smaller ($12.1 \pm 5.1\%$) and appeared later than controls (Fig. 1e,f and Supplementary Fig. S1d). We conclude that, in the absence of cortical flows, PAR-2 loading depends on microtubules and correlates spatially and temporally with MTOC–cortex contact.

Enrichment of PAR-2 on the MTOC core during symmetry breaking raised the possibility that PAR-2 has microtubule-binding activity. We found that recombinant PAR-2 could be pelleted with, but not without, microtubules by high-speed centrifugation (apparent dissociation constant, K_d: 1.19 μM, Fig. 2b and Supplementary Fig. S2). Visualization of recombinant GFP::PAR-2 mixed with rhodamine-labelled microtubules confirmed that PAR-2 binds microtubules *in vitro* (Fig. 2c). Deletion analysis identified three microtubule-binding regions in PAR-2 (Fig. 2a and Supplementary Fig. S3a). A fusion (GFP::PAR-2(1–221)) containing the first microtubule-binding region but lacking the cortical-localization domain localized to spindles *in vivo* (Supplementary Fig. S3a). Full-length GFP::PAR-2 also localized to spindles, but only in zygotes treated with the microtubule-

[1]Department of Molecular Biology and Genetics, Howard Hughes Medical Institute, Center for Cell Dynamics, Johns Hopkins University School of Medicine, 725 N. Wolfe St., PCTB 706, Baltimore, Maryland 21205, USA.
[2]Correspondence should be addressed to G.S. (e-mail: gseydoux@jhmi.edu)

Received 11 May 2011; accepted 5 September 2011; published online 9 October 2011; DOI: 10.1038/ncb2354

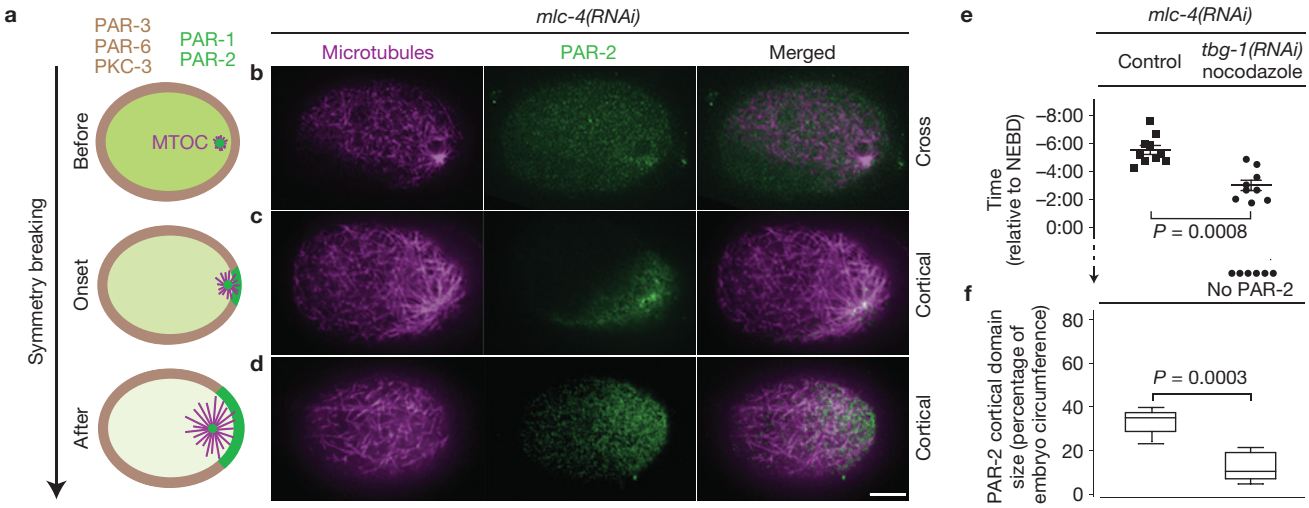

Figure 1 PAR-2 dynamics at symmetry breaking. (**a**) Schematic representation of an embryo showing the distribution of PAR-1 and PAR-2 (green), anterior PARs (brown) and MTOC microtubules (magenta). Zygotes are oriented with the posterior to the right in this and all figures. (**b**–**d**) Confocal microscopy images of fixed *mlc-4(RNAi)* zygotes stained for tubulin (magenta) and PAR-2 (green). Note that **b** shows a cross-section as in the schematic representations in **a**, whereas **c** and **d** show superficial cortical sections. Scale bar, 10 μm. (**e**) The timing of GFP::PAR-2 appearance on the posterior cortex in live *mlc-4(RNAi)* zygotes relative to nuclear envelope breakdown (NEBD). Each dot represents an individual zygote. 'No PAR-2' refers to zygotes for which PAR-2 never loaded on the cortex. '*tbg-1(RNAi)* nocodazole' refers to zygotes depleted for γ-tubulin and treated with nocodazole. Error bars represent s.d. from 10 control zygotes and 9 *tbg-1(RNAi)* nocodazole zygotes with a cortical GFP::PAR-2 domain. (**f**) Graph showing the size of the GFP::PAR-2 domain scored at nuclear envelope breakdown. Error bars represent s.d. in zygotes with a cortical GFP::PAR-2 domain as in **e**. See Supplementary Fig. S1d for images of zygotes used to compile data in **e** and **f**.

stabilizing drug taxol (Supplementary Fig. S3b). Mutagenesis of basic residues conserved in *C. briggsae* and *C. remanei* PAR-2 yielded two mutations (R163A and R183–5A) that significantly decreased the level of microtubule binding *in vitro* (Fig. 2a–c and Supplementary Figs S2 and S4). R183–5A also interfered with the localization of GFP::PAR-2(1–221) to spindles (Supplementary Fig. S3a), and with the localization of full-length PAR-2 to taxol-stabilized spindles (Supplementary Fig. S3b), and to the MTOC at symmetry breaking (Supplementary Fig. S1b). We conclude that the first microtubule-binding domain of PAR-2 is necessary and sufficient for interactions with microtubules *in vitro* and *in vivo*, and that microtubule binding is required to enrich PAR-2 on the MTOC core during symmetry breaking.

To determine the function of microtubule binding, we expressed GFP::PAR-2^{R163A} and GFP::PAR-2$^{R183–5A}$ from RNA interference (RNAi)-resistant transgenes in *mlc-4(RNAi)* zygotes depleted of endogenous PAR-2 (see Methods). For positive controls, we used wild-type GFP::PAR-2 and a mutation (K162A) in the first microtubule-binding domain that does not affect microtubule-binding affinity *in vitro* (Fig. 2b and Supplementary Fig. S2). All fusions were expressed at comparable levels (Supplementary Fig. S5a). Whereas GFP::PAR-2 and GFP::PAR-2^{K162A} localized to the posterior cortex, GFP::PAR-2^{R163A} and GFP::PAR-2$^{R183–5A}$ remained in the cytoplasm in most zygotes (Fig. 3a and Supplementary Table S1). We obtained identical results under three other conditions that eliminate MTOC-induced cortical flows: *ect-2(ax751)* (ref. 4), *mat-1(ax227)* (ref. 7) and *spd-5(RNAi)* (ref. 8; Fig. 3a and Supplementary Table S1). Localization to the cortex was restored by decreasing the level of PKC-3 by RNAi or by eliminating the PKC-3 phosphorylation sites in PAR-2 (Fig. 3a and Supplementary Table S1). GFP::PAR-2 and GFP::PAR-2$^{R183–5A}$ exhibited identical cortical dynamics in *pkc-3(RNAi)* zygotes, as revealed by fluorescence recovery after photobleaching (FRAP; Fig. 3b and Supplementary Fig. S5b). GFP::PAR-2^{R163A} and GFP::PAR-2$^{R183–5A}$ localized to the posterior cortex in *mlc-4(+)* embryos (in which PKC-3 is mobilized by flows; Fig. 3a) and could rescue the embryonic lethality of *par-2(RNAi)* and/or *par-2(lw32)* zygotes to the same extent as wild-type GFP::PAR-2 (Supplementary Table S2). We conclude that microtubule binding is essential for symmetry breaking but not for polarity maintenance, or for PAR-2 to associate with the cortex in the absence of PKC-3.

The microtubule-binding regions of PAR-2 contain several PKC-3 phosphorylation sites (Fig. 2a), raising the possibility that microtubule binding protects PAR-2 from phosphorylation by PKC-3. Consistent with this possibility, the addition of microtubules inhibited the phosphorylation of PAR-2 by human aPKC *in vitro* (Fig. 2d and Supplementary Fig. S6a). Inhibition was not observed in the presence of nocodazole (Supplementary Fig. S6b), or when the PAR-2 microtubule-binding mutants (R163A and R183–5A) were used as substrates (Fig. 2d and Supplementary Fig. S6a). Consistent with microtubules acting as competitive inhibitors, 0.8 μM polymerized tubulin was sufficient to increase the Michaelis constant (K_m) by 65% without affecting the maximum velocity (V_{max}) of the aPKC kinase reaction (Supplementary Fig. S6c). The average intracellular tubulin concentration has been estimated at ~20 μM (ref. 9) and should be even higher at the MTOC core, consistent with the possibility that microtubules protect PAR-2 from PKC-3 at symmetry breaking.

To test this hypothesis further, we developed an *in vitro* microtubule/PKC-3 competition assay in the presence of a 'cortex mimic'. Interactions with plasma membrane phospholipids have been implicated in the localization of PAR-1 and PAR-3 homologues to the cortex[10,11]. Using a protein–lipid binding assay, we found that PAR-2 interacts with phospholipids including phosphoinositides (Fig. 2e,f and

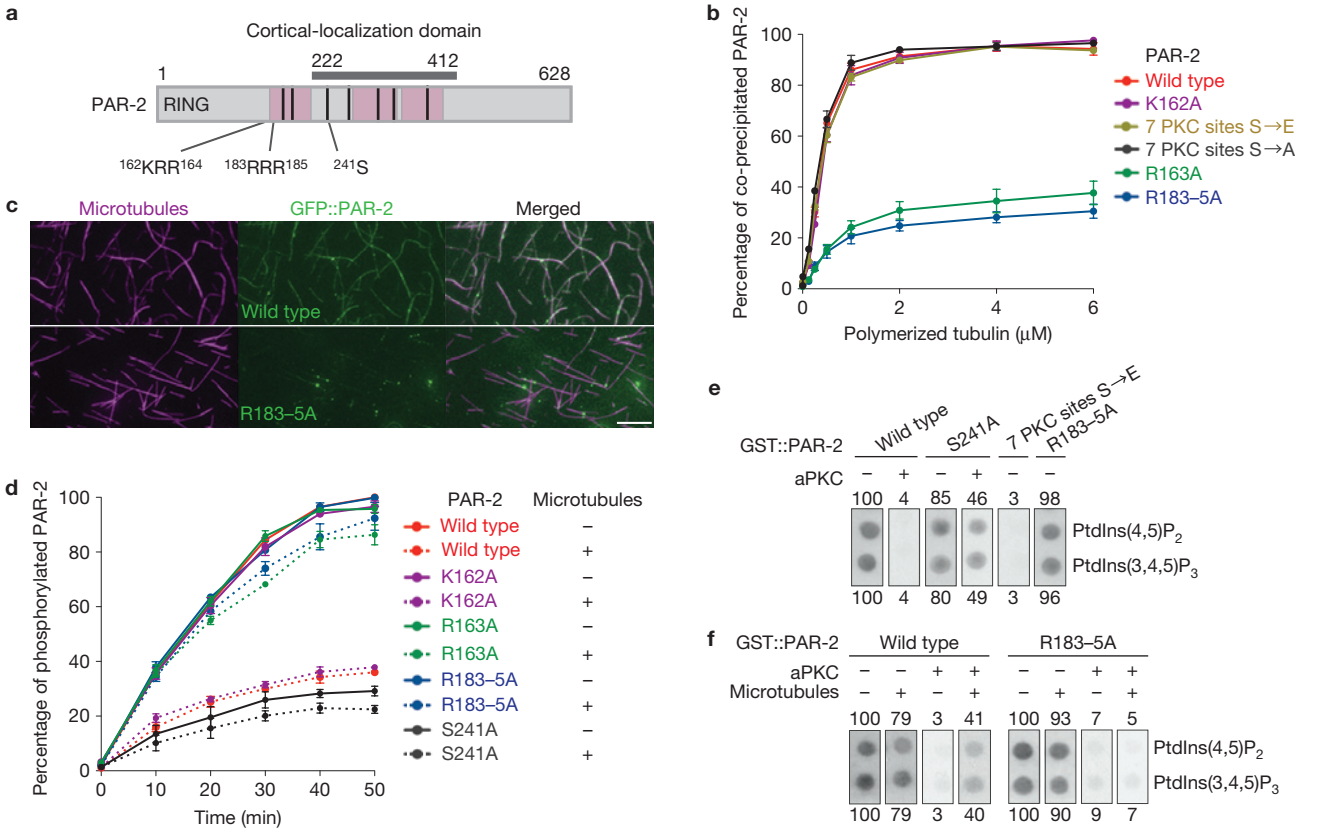

Figure 2 Microtubule binding protects PAR-2 from aPKC phosphorylation and allows PAR-2 to interact with phospholipids in the presence of aPKC. (**a**) Schematic representation of PAR-2. The pink areas are regions that contribute to microtubule binding *in vitro* (see Supplementary Fig. S3a). The cortical-localization domain is the region sufficient for localization to the posterior cortex in the presence of endogenous PAR-2 (ref. 12 and F. Motegi, unpublished observation). The black bars indicate seven potential PKC-3 phosphorylation sites[12]. Ser 241 is required for maximal phosphorylation *in vitro* by aPKC (**d**) and for cortical exclusion *in vivo* (Fig. 3a). ^{162}KRR^{164} is the basic cluster mutated in the single-substitution mutants K162A and R163A, and ^{183}RRR^{185} is the basic cluster mutated in the triple-substitution mutant R183–5A. (**b**) Percentage of recombinant PAR-2 that co-sedimented with microtubules. Error bars represent s.d. of three independent experiments. (**c**) Photomicrographs of recombinant GFP::PAR-2 mixed with rhodamine-labelled microtubules and spread on slides. GFP::PAR-2$^{R183–5A}$ does not label microtubules as efficiently as wild-type GFP::PAR-2. Scale bar, 5 μm. (**d**) Percentage of phosphorylated PAR-2 with respect to time from the start of incubation with aPKC kinase in the presence (dotted lines) or absence (solid lines) of microtubules. PAR-2 phosphorylation was monitored by [γ-^{32}P]ATP incorporation. Error bars represent s.d. of three independent experiments. (**e**) Phosphorylation by aPKC inhibits PAR-2 binding to phospholipids. GST::PAR-2 fusions pre-treated with or without aPKC were incubated with lipid strips and detected using an anti-GST antibody. Phosphatidylinositol-4,5-bisphosphate (PtdIns(4,5)P_2) and Phosphatidylinositol-3,4,5-trisphosphate (PtdIns(3,4,5)P_3) 50-pmol spots are shown (see Supplementary Fig. S7b for the full dilution series). The numbers represent the percentage of binding normalized to wild type (100%). Ser 241 is one of seven predicted aPKC sites. '7 PKC sites S → E' is a phosphomimic mutant for all seven sites. (**f**) Binding to microtubules is sufficient to protect PAR-2 from aPKC and retain binding to phospholipids. The same as in **e**, but GST::PAR-2 fusions were incubated with microtubules before incubation with aPKC. See Supplementary Fig. S7c for the full dilution series.

Supplementary Fig. S7). Phosphorylation by aPKC, or phosphomimetic mutations in the PKC-3 sites, interfered with PAR-2 binding to lipids (Fig. 2e,f and Supplementary Fig. S7), as they interfere with PAR-2 cortical-localization *in vivo*[12]. Remarkably, pre-incubation with 1.5 μM polymerized tubulin rescued the ability of PAR-2 to bind to lipids in the presence of aPKC (Fig. 2f and Supplementary Fig. S7c). Microtubules did not restore lipid binding to PAR-2$^{R183–5A}$ (Fig. 2f and Supplementary Fig. S7c), even though this mutant could bind lipids as efficiently as wild-type PAR-2 in the absence of aPKC (Fig. 2e and Supplementary Fig. S7a,b). We conclude that binding to microtubules is sufficient to protect PAR-2 from aPKC PKC-3 and retain binding to plasma membrane lipids.

After reaching the cortex, PAR-2 becomes partially resistant to exclusion by PKC-3, and this resistance depends on the PAR-2 RING domain[12]. FRAP analyses revealed faster cortical dynamics for the RING mutant GFP::PAR-2^{C56S} when compared with GFP::PAR-2 and GFP::PAR-2$^{R183–5A}$ (Fig. 3b and Supplementary Fig. S5b). GFP::PAR-2^{C56S} was enriched on the MTOC at the time of MTOC–cortex contact in most *mlc-4(RNAi)* zygotes (14 of 25), but did not form a posterior cortical domain (Fig. 3c and Supplementary Fig. S1b). Endogenous PAR-2 could rescue the cortical-localization of both GFP::PAR-2^{C56S} and GFP::PAR-2$^{R183–5A}$ in *mlc-4(RNAi)* zygotes (Fig. 3c). These results indicate that cortical PAR-2 is stabilized at the cortex by its RING domain, and recruits additional PAR-2 molecules from the cytoplasm independently of microtubule binding.

By pronuclear meeting, PAR-3 and PKC-3 were excluded from the PAR-2 domain (Fig. 4a and Supplementary Table S3). This exclusion was dependent on PAR-1 (Fig. 4a and Supplementary Table S3). PAR-1 co-localized with PAR-2 on the posterior cortex in *mlc-4(RNAi)* zygotes expressing wild-type GFP::PAR-2, but not in zygotes expressing GFP::PAR-2$^{R183–5A}$, in which PAR-2 does not load and PAR-3 and PKC-3 are not excluded (Fig. 4a and Supplementary Table S3). In

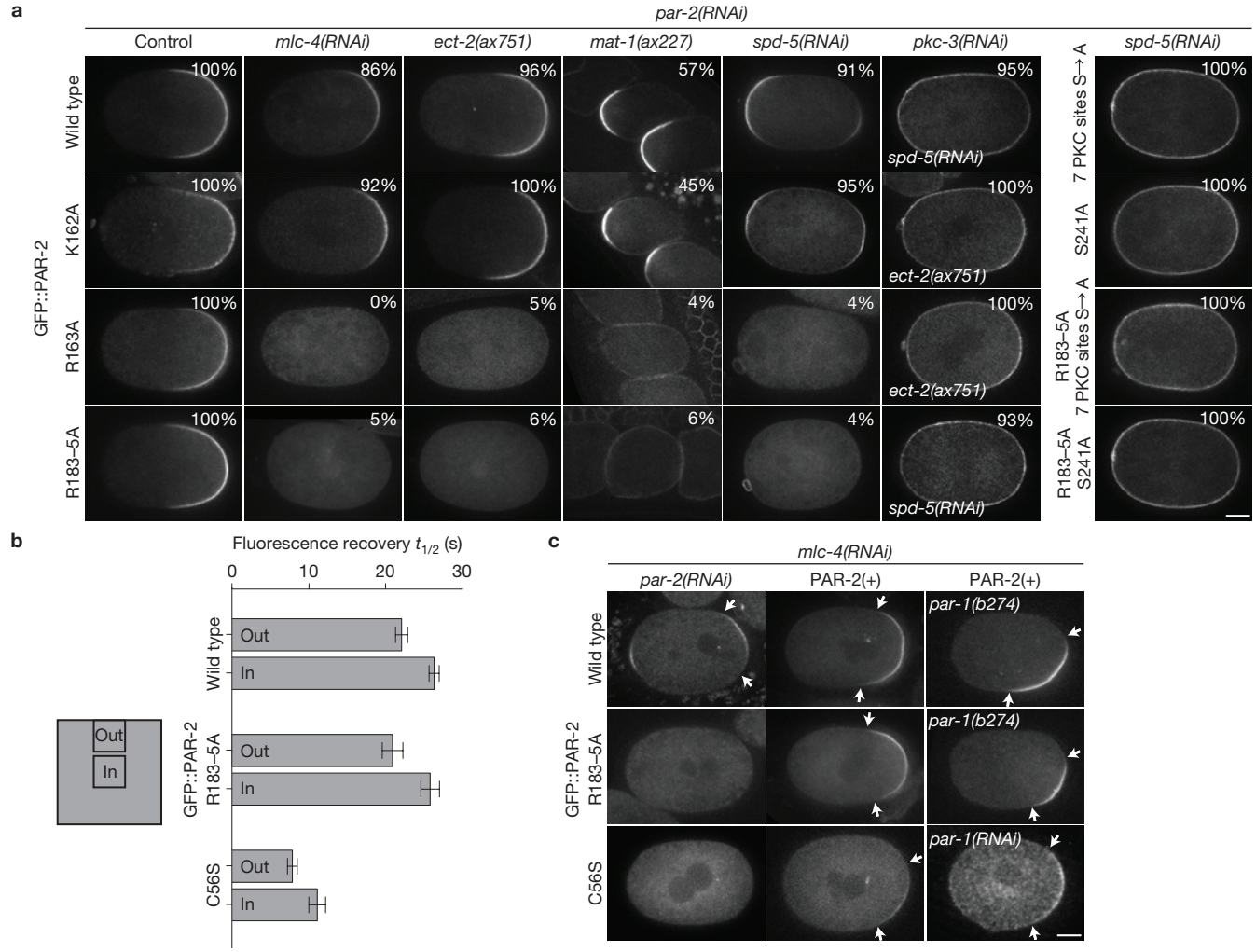

Figure 3 Microtubule binding is required for PAR-2 to localize to the cortex in the absence of cortical flows. (**a**) Live zygotes expressing the indicated GFP::PAR-2 fusions: wild type and K162A bind microtubules, whereas R163A and R183–5A do not. The percentages indicate zygotes with cortical PAR-2; numbers are presented in Supplementary Table S1. ECT-2 is the GEF for the small GTPase RHO-1 (ref. 29). *ect-2(ax751)* zygotes lack MTOC-induced cortical flows, but develop PAR-2-dependent cortical flows during mitosis[4]. MAT-1 is a subunit of the anaphase-promoting complex. *mat-1(ax227)* zygotes arrest in meiosis and become transiently polarized without cortical flows under the influence of the acentriolar meiotic spindle[7]. SPD-5 is a MTOC component required for PCM assembly[8]. *spd-5(RNAi)* zygotes localize GFP::PAR-2 to both the anterior and posterior cortex under the influence of the meiotic spindle remnant (anterior) and the slow-maturing MTOC (posterior)[18]. RNAi depletion of PKC-3 or mutations in the PKC phosphorylation sites (either 7 PKC sites S → A or S241A) cause all fusions to localize uniformly to the cortex. Scale bar, 10 μm. (**b**) FRAP was carried out on the cortex of *pkc-3(RNAi)* zygotes expressing the indicated GFP::PAR-2 fusions. The graph shows the average recovery half-time ($t_{1/2}$) from five separate zygotes. Error bars represent s.d. Fluorescence recovery was faster at the boundary (Out) than at the centre (In) of the bleached area, indicating that at least some of the recovery is due to lateral diffusion of cortical GFP::PAR-2, as shown in ref. 26 (schematic representation of bleached area is shown on the left, with areas in which recovery was measured as indicated). See Supplementary Fig. S5b for representative recovery curves. (**c**) Cortical PAR-2 stimulates its own recruitment to the cortex. Live zygotes expressing the indicated GFP::PAR-2 fusions. The arrows point to the boundaries of the cortical GFP::PAR-2 domain. Scale bar, 10 μm. In *mlc-4(RNAi);par-2(RNAi)* zygotes, wild-type PAR-2 localizes to the posterior cortex, but the microtubule-binding mutant R183–5A and the RING mutant C56S do not. Endogenous PAR-2 (PAR-2(+)) rescues the localization of both mutants. Rescue is also observed in *par-1 (RNAi)* and *par-1* mutant zygotes, in which PAR-3 and PKC-3 are never excluded from the posterior cortex (see Fig. 4a).

Drosophila oocytes, PAR-1 phosphorylates PAR-3, causing PAR-3 to lose its cortical association[13]. *In vitro* kinase assays confirmed that *C. elegans* PAR-1 can phosphorylate PAR-3 (Supplementary Fig. S8a,b). Furthermore, we found that PAR-3 and PKC-3 were not excluded in zygotes in which PAR-1 lacked kinase activity[14] or its cortical-localization domain[15], or in zygotes expressing a PAR-3 fusion missing the PAR-1 phosphorylation sites[16] (Fig. 4a and Supplementary Table S3). We conclude that recruitment of PAR-1 to the PAR-2 domain leads to exclusion of the PAR-3–PKC-3 complex, probably by direct phosphorylation of PAR-3 by PAR-1.

In mammalian cells, PAR-1 cortical-localization depends on a carboxy-terminal domain that contains a conserved aPKC phosphorylation site required for cortical exclusion by aPKC (ref. 17). We confirmed that the corresponding domain of *C. elegans* PAR-1 (amino acids 965–1192) is necessary and sufficient to target PAR-1 to the cortex (Supplementary Fig. S8c), and that the conserved aPKC site Thr 983 can be phosphorylated by aPKC *in vitro* (Supplementary Fig. S8d) and is required to exclude PAR-1 from PKC-3(+) cortices *in vivo* (Supplementary Fig. S8c). Remarkably, we found that GFP::PAR-1(965–1192 aa) and PAR-1(*it51*), which

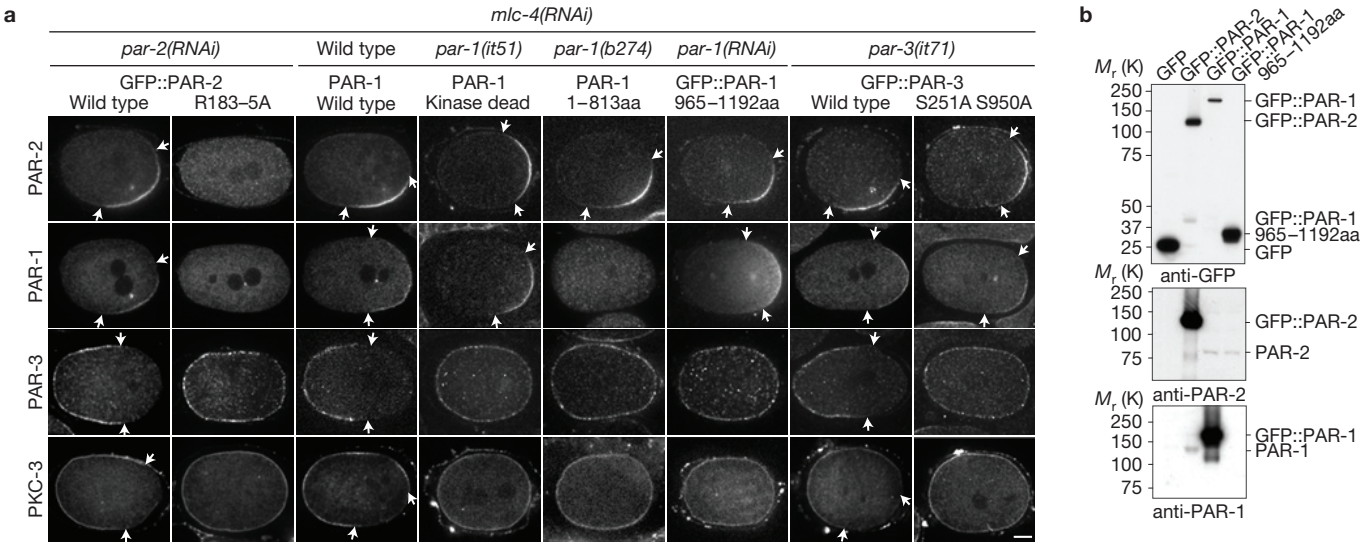

Figure 4 PAR-2 recruits PAR-1 to the cortex, leading to exclusion of anterior PARs. (**a**) *mlc-4(RNAi)* zygotes with indicated mutations in PAR proteins stained for PAR-2, PAR-1, PAR-3 and PKC-3. *par-1(it51)* contains a mutation (R409K) that inhibits kinase activity[14], and *par-1(b274)* contains a premature stop (Q814Stop) that eliminates the PAR-1 cortical-localization domain[15]. GFP::PAR-3$^{S251A\ S950A}$ contains mutations in the conserved PAR-1 phosphorylation sites and rescues *par-3(it71)* zygotes competent for cortical flows[16]. GFP::PAR-2 fusions were co-stained with PAR-1. PAR-2 and PKC-3 or PAR-1 and PAR-3 were co-stained in the other zygotes. The arrows indicate the boundary of the PAR domains. Scale bar, 10 μm. (**b**) Immunoprecipitation experiment showing that PAR-2 and PAR-1 interact in embryo extracts. Extracts from embryos expressing the indicated GFP fusions were immunoprecipitated with anti-GFP beads and the immunoprecipitates were blotted with the indicated antibodies.

cannot exclude PAR-3 and PKC-3, were still able to localize with PAR-2 on the posterior cortex in *mlc-4(RNAi)* zygotes (Fig. 4a and Supplementary Table S3), indicating that PAR-2 can recruit PAR-1 to cortices also occupied by PKC-3. To determine whether PAR-1 and PAR-2 interact, we first immunoprecipitated GFP::PAR-1 and GFP::PAR-2 from worm extracts. We detected endogenous PAR-2 in GFP::PAR-1 immunoprecipitates and endogenous PAR-1 in GFP::PAR-2 immunoprecipitates, indicating that at least a subset of PAR-2 and PAR-1 molecules are in a complex (Fig. 4b). Using purified recombinant proteins, we found that PAR-1 and PAR-2 interact directly, and that the PAR-1 C terminus is sufficient for the interaction (Supplementary Fig. S8e). We conclude that PAR-2 recruits PAR-1 to the cortex, through a direct interaction involving the PAR-1 C-terminal domain.

In wild-type embryos, depletion of tubulin delays symmetry breaking[18], raising the possibility that microtubule-dependent loading of PAR-2 contributes to symmetry breaking even in the presence of flows. Consistent with this possibility, at symmetry breaking, GFP::PAR-2$^{R183-5A}$ zygotes showed either a uniform PAR-3 distribution and no PAR-2 at the cortex (2 of 12), or an asymmetric PAR-3 distribution and no (5 of 12) or low levels of PAR-2 (5 of 12). In contrast, 9 of 10 zygotes expressing wild-type GFP::PAR-2 already had complementary PAR-2/PAR-3 domains at this stage (Fig. 5a). Live-cell imaging experiments revealed that GFP::PAR-2$^{R183-5A}$ loads on the posterior cortex 29.0 ± 11.2 s later than GFP::PAR-2 (Fig. 5b). After this initial delay, GFP::PAR-2$^{R183-5A}$ cortical levels increased rapidly and were indistinguishable from GFP::PAR-2 levels by mitosis (Fig. 5a,b), and all zygotes fixed at this stage excluded PAR-3 from the GFP::PAR-2 domain (Fig. 5a). We conclude that, in wild-type embryos, microtubule binding by PAR-2 contributes to the fast kinetics of PAR-2 loading/PAR-3 clearing, but is not essential after cortical flows displace anterior PARs.

Our observations support a simple model for polarization of the *C. elegans* zygote (Fig. 5c). When the MTOC contacts the cortex, the high density of microtubules transiently protects PAR-2 from phosphorylation by PKC-3, allowing a few molecules of unphosphorylated PAR-2 to interact productively with the cortex. Cortical PAR-2, stabilized by its RING domain, recruits PAR-1 as well as additional PAR-2 molecules ('PAR-2 feedback loop'), allowing the PAR-2/PAR-1 domain to expand beyond the site of MTOC–cortex contact. PAR-1 phosphorylates PAR-3, causing the PAR-3–PKC-3 complex to leave the cortex. The anterior PARs are also displaced by cortical flows triggered by the MTOC. Both symmetry-breaking functions of the MTOC (induction of cortical flows and protection of PAR-2 from PKC-3) are transient and depend on the PAR-2 feedback loop and PAR-1 for PAR domain maintenance (also see ref. 12).

This model clarifies several observations in the literature. First, although some studies support a role for microtubules in symmetry breaking[7,18], others have indicated that microtubules are not required[19,20]. Our findings demonstrate a role for microtubules to load PAR-2 at the earliest stage of symmetry breaking, but leave open the possibility that the MTOC uses a second, microtubule-independent cue to initiate cortical flows[21]. Our model also explains why PAR-2 is not essential to exclude anterior PARs in *par-6*/+ zygotes[22,23] or zygotes that overexpress LGL-1, which, similarly to PAR-1, antagonizes the cortical-localization of anterior PARs (refs 24,25). We suggest that the primary function of the PAR-2 feedback loop is to maintain sufficient PAR-1 on the posterior cortex to ensure permanent exclusion of anterior PARs. This function may not be needed in embryos in which cortical levels of anterior PARs are already biased by flows and further decreased by mutation or LGL-1 overexpression. A remaining question is what prevents the PAR-2 domain from spreading to the entire cortex. Anterior and posterior PARs exchange with the cytoplasm and diffuse freely across the PAR boundary[26]. One possibility, therefore,

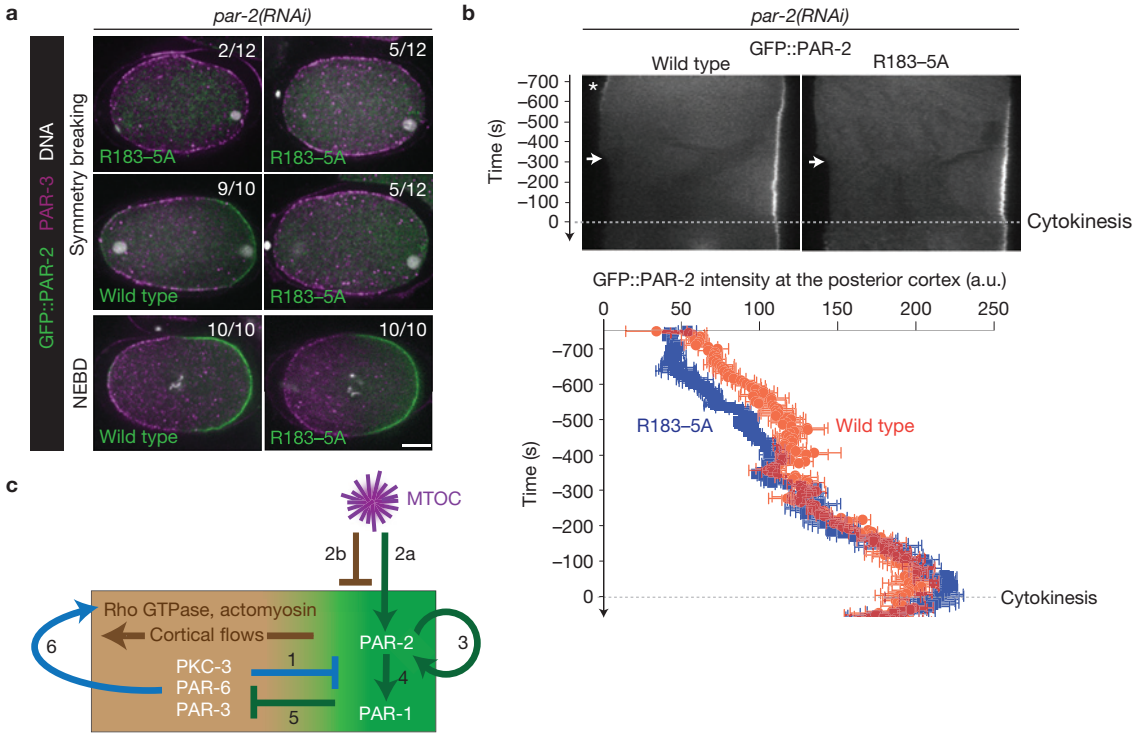

Figure 5 Microtubule binding by PAR-2 is required for efficient polarity initiation in wild-type embryos. (**a**) Fluorescence micrographs of fixed zygotes expressing GFP::PAR-2 and depleted for endogenous PAR-2 by RNAi. Zygotes are stained for GFP::PAR-2 (green), PAR-3 (magenta) and DNA (white) and are shown at symmetry breaking (top two rows) or at nuclear envelope breakdown (NEBD; bottom row). Scale bar, 10 μm. (**b**) Top, kymographs from time-lapse movies of live zygotes expressing GFP::PAR-2 fusions and depleted for endogenous PAR-2 by RNAi. Times are with respect to the onset of cytokinesis. Wild-type GFP::PAR-2 appears on the posterior cortex earlier than the microtubule-binding mutant GFP::PAR-2$^{R183-5A}$. Wild-type GFP::PAR-2 also accumulates transiently (asterisk) on the anterior cortex (owing to the transient influence of the meiotic spindle remnant[18]; 5 of 5 zygotes). GFP::PAR-2$^{R183-5A}$ does not show this localization (0 of 5), consistent with polarization by the meiotic spindle depending primarily on microtubules[7]. Bottom, the graph shows the fluorescence intensity at the posterior-most cortex averaged from five zygotes. Accumulation of GFP::PAR-2$^{R183-5A}$ is delayed when compared with wild-type GFP::PAR-2 (29.0 ± 11.2 s, $P = 0.03$) but catches up by nuclear envelope breakdown. Error bars represent s.d. from five separate zygotes. (**c**) Model for polarization of the *C. elegans* zygote. 1, PKC-3 phosphorylates PAR-2 (ref. 12) and PAR-1, keeping them off the cortex. 2, MTOC breaks symmetry through two parallel mechanisms: 2a, microtubules at the MTOC protect PAR-2 from phosphorylation by PKC-3, allowing a few molecules of PAR-2 to load on the cortex close to MTOC; 2b, MTOC induces cortical flows by an unknown mechanism involving local inhibition of actomyosin[3]. Flows displace anterior PARs, allowing PAR-2 to accumulate in their place. 3, Cortical PAR-2 recruits additional PAR-2 molecules to expand the PAR-2 domain. The RING finger of PAR-2 stabilizes PAR-2 at the cortex. 4, PAR-2 recruits PAR-1 by binding to the C terminus of PAR-1. 5, PAR-1 phosphorylates PAR-3 preventing its association with the cortex. 6, Anterior PARs stimulate their own displacement by recruiting myosin to the cortex and upregulating cortical flows[3,4]. Not shown in this figure is LGL, a non-essential player in this process, which similarly to PAR-1 localizes to the posterior cortex and antagonizes the cortical association of anterior PARs (refs 24,25).

is that as the anterior PARs become restricted to a smaller region of the cortex, the concentration of PKC-3 at the boundary reaches a threshold sufficient to block further PAR-2 spreading.

The PAR system has been implicated in the polarization of several cell types, including some that do not undergo cortical flows[27]. Our findings illustrate how the self-organizing properties of the PAR network are sufficient to polarize a cell in the absence of long-range actin dynamics. In principle, any localized cue that favours the binding of one class of PARs with the cortex will be sufficient to initiate a cascade of self-organizing interactions within the network. We suggest that cortical flows, although non-essential, contribute to the polarization process by increasing the robustness of the response. Cortical flows may also serve to align PAR asymmetry with the cell's intrinsic geometry, as PAR domains are often misaligned with respect to the long axis of *mlc-4(RNAi)* zygotes[4] (Fig. 4a).

Microtubules have been proposed to polarize cells by transporting polarity regulators to specific regions of the cell (reviewed in ref. 28). Our findings identify another way in which microtubules break symmetry: by protecting polarity regulators from cortical exclusion by aPKC. □

METHODS

Methods and any associated references are available in the online version of the paper at http://www.nature.com/naturecellbiology

Note: Supplementary Information is available on the Nature Cell Biology website

ACKNOWLEDGEMENTS

This study was supported by the Japan Society for the Promotion of Science (F.M.), the American Cancer Society (PF-08-158-01; E.G.) and the National Institute of Health (R01HD37047; G.S.). G.S. is an investigator of the Howard Hughes Medical Institute. We thank J. Ahringer, A. Audhya, L. Boyd, A. Desai, P. Gonczy, M. Gotta, R. Green, C. Hoege, K. Kemphues, Y. Nishimura, K. F. O'Connell, K. Oegema, L. S. Rose, A. Sugimoto, C. M. Waterman, H. Zaher and the *Caenorhabditis* Genetic Center for reagents and expertise.

AUTHOR CONTRIBUTIONS

F.M. and G.S. designed the study and wrote the manuscript. S.Z. carried out experiments shown in Fig. 3b and Supplementary Fig. S5b, Y.H. A.A.C. and E.G. carried out experiments shown in Supplementary Fig. S8c,d and F.M. carried out all other experiments.

COMPETING FINANCIAL INTERESTS

The authors declare no competing financial interests.

Published online at http://www.nature.com/naturecellbiology
Reprints and permissions information is available online at http://www.nature.com/reprints

1. Goldstein, B. & Macara, I. The PAR proteins: fundamental players in animal cell polarization. *Dev. Cell* **13,** 609–622 (2007).
2. St Johnston, D. & Ahringer, J. Cell polarity in eggs and epithelia: parallels and diversity. *Cell* **141,** 757–774 (2010).
3. Munro, E., Nance, J. & Priess, J. R. Cortical flows powered by asymmetrical contraction transport PAR proteins to establish and maintain anterior–posterior polarity in the early *C. elegans* embryo. *Dev. Cell* **7,** 413–424 (2004).
4. Zonies, S., Motegi, F., Hao, Y. & Seydoux, G. Symmetry breaking and polarization of the *C. elegans* zygote by the polarity protein PAR-2. *Development* **137,** 1669–1677 (2010).
5. Cuenca, A. A., Schetter, A., Aceto, D., Kemphues, K. & Seydoux, G. Polarization of the *C. elegans* zygote proceeds via distinct establishment and maintenance phases. *Development* **130,** 1255–1265 (2003).
6. Shelton, C., Carter, J., Ellis, G. & Bowerman, B. The nonmuscle myosin regulatory light chain gene mlc-4 is required for cytokinesis, anterior–posterior polarity, and body morphology during *Caenorhabditis elegans* embryogenesis. *J. Cell Biol.* **146,** 439–451 (1999).
7. Wallenfang, M. R. & Seydoux, G. Polarization of the anterior–posterior axis of *C. elegans* is a microtubule-directed process. *Nature* **408,** 89–92 (2000).
8. Hamill, D. R., Severson, A. F., Carter, J. C. & Bowerman, B. Centrosome maturation and mitotic spindle assembly in *C. elegans* require SPD-5, a protein with multiple coiled-coil domains. *Dev. Cell* **3,** 673–684 (2002).
9. Hiller, G. & Weber, K. Radioimmunoassay for tubulin: a quantitative comparison of the tubulin content of different established tissue culture cells and tissues. *Cell* **14,** 795–804 (1978).
10. Moravcevic, K. *et al.* Kinase associated-1 domains drive MARK/PAR1 kinases to membrane targets by binding acidic phospholipids. *Cell* **143,** 966–977 (2010).
11. Wu, H. *et al.* PDZ domains of Par-3 as potential phosphoinositide signaling integrators. *Mol. Cell* **28,** 886–898 (2007).
12. Hao, Y., Boyd, L. & Seydoux, G. Stabilization of cell polarity by the *C. elegans* RING protein PAR-2. *Dev. Cell* **10,** 199–208 (2006).
13. Benton, R. & St Johnston, D. *Drosophila* PAR-1 and 14-3-3 inhibit Bazooka/PAR-3 to establish complementary cortical domains in polarized cells. *Cell* **115,** 691–704 (2003).
14. Guo, S. & Kemphues, K. par-1, a gene required for establishing polarity in *C. elegans* embryos, encodes a putative Ser/Thr kinase that is asymmetrically distributed. *Cell* **81,** 611–620 (1995).
15. Griffin, E., Odde, E. & Seydoux, G. Regulation of the MEX-5 gradient by a spatially segregated kinase/phosphatase cycle. *Cell* **146,** 955–968 (2011).
16. Li, B., Kim, H., Beers, M. & Kemphues, K. Different domains of *C. elegans* PAR-3 are required at different times in development. *Dev. Biol.* **344,** 745–757 (2010).
17. Matenia, D. & Mandelkow, E. M. The tau of MARK: a polarized view of the cytoskeleton. *Trends Biochem. Sci.* **34,** 332–342 (2009).
18. Tsai, M. C. & Ahringer, J. Microtubules are involved in anterior–posterior axis formation in *C. elegans* embryos. *J. Cell Biol.* **179,** 397–402 (2007).
19. Cowan, C. R. & Hyman, A. A. Centrosomes direct cell polarity independently of microtubule assembly in *C. elegans* embryos. *Nature* **431,** 92–96 (2004).
20. Sonneville, R. & Gonczy, P. zyg-11 and cul-2 regulate progression through meiosis II and polarity establishment in *C. elegans*. *Development* **131,** 3527–3543 (2004).
21. Jenkins, N., Saam, J. R. & Mango, S. E. CYK-4/GAP provides a localized cue to initiate anteroposterior polarity upon fertilization. *Science* **313,** 1298–1301 (2006).
22. Watts, J. *et al.* par-6, a gene involved in the establishment of asymmetry in early *C. elegans* embryos, mediates the asymmetric localization of PAR-3. *Development* **122,** 3133–3140 (1996).
23. Labbé, J. C., Pacquelet, A., Marty, T. & Gotta, M. A genomewide screen for suppressors of par-2 uncovers potential regulators of PAR protein-dependent cell polarity in *Caenorhabditis elegans*. *Genetics* **174,** 285–295 (2006).
24. Hoege, C. *et al.* LGL can partition the cortex of one-cell *Caenorhabditis elegans* embryos into two domains. *Curr. Biol.* **20,** 1296–1303 (2010).
25. Beatty, A., Morton, D. & Kemphues, K. The *C. elegans* homolog of *Drosophila* Lethal giant larvae functions redundantly with PAR-2 to maintain polarity in the early embryo. *Development* **137,** 3995–4004 (2010).
26. Goehring, N. W., Hoege, C., Grill, S. W. & Hyman, A. A. PAR proteins diffuse freely across the anterior–posterior boundary in polarized *C. elegans* embryos. *J. Cell Biol.* **193,** 583–594 (2011).
27. Doerflinger, H. *et al.* Bazooka is required for polarisation of the *Drosophila* anterior–posterior axis. *Development* **137,** 1765–1773 (2010).
28. Siegrist, S. E. & Doe, C. Q. Microtubule-induced cortical cell polarity. *Genes Dev.* **21,** 483–496 (2007).
29. Morita, K., Hirono, K. & Han, M. The *Caenorhabditis elegans* ect-2 RhoGEF gene regulates cytokinesis and migration of epidermal P cells. *EMBO Rep.* **6,** 1163–1168 (2005).

DOI: 10.1038/ncb2354

METHODS

Worm strains and transgenics. Transgenes were constructed in the pID3.01 Gateway destination vector[30] and transformed into worms by biolistic transformation[31]. Base pairs 6–523 of *par-2* were recoded to create the RNAi-resistant *par-2* transgene. The following strains were used: N2 (wild type), *axIs1932* (pFM032, *gfp::par-2*), *axIs1933* (pFM034, *gfp::par-2*$^{RNAi\text{-}resistant}$), *axIs1934* (pFM035, *gfp::par-2*$^{RNAi\text{-}resistant}$ *(R183–5A))*, *axIs1935* (pFM036, *gfp::par-2*$^{RNAi\text{-}resistant}$ *(K162A))*, *axIs1936* (pFM037, *gfp::par-2*$^{RNAi\text{-}resistant}$ *(R163A))*, *axIs1937* (pFM038, *gfp::par-2*$^{RNAi\text{-}resistant}$ *(R183–5A+7SA))*, *axIs1938* (pFM039, *gfp::par-2*$^{RNAi\text{-}resistant}$ *(R183–5A+S241A))*, *axIs1939* (pFM040, *gfp::par-2*$^{RNAi\text{-}resistant}$ *(7SA))*, *axIs1945* (pFM041, *gfp::par-2*$^{RNAi\text{-}resistant}$*(S241A))*, *axIs1949* (pSZ61, *gfp::par-2*$^{RNAi\text{-}resistant}$ *(C56S))*, *axIs1944* (pFM051, *mCherry::tba-2*), *axIs1245* (pAC2.01, *gfp::par-1*), *axIs1947* (pYH3.24; *gfp::par-1*$^{1\text{–}964}$), *axIs1327* (pAC1.08, *gfp::par-1*$^{965\text{–}1192}$), *axIs1948* (pYH3.31; *gfp::par-1(K199A))*, *axIs1949* (pYH3.31; *gfp::par-1 K199A T983A*), *axIs1412* (pAC2.03; *gfp:par-1*$^{965\text{–}1192}$*(T983A))*, *axIs1374* (*gfp*), *itIs174* (*Ppar-3::par-3::gfp*) (ref. 16), *itIs234* (*Ppar-3::par3(S251A S950A)::gfp*) (ref. 16), *ltIs44* (*mCherry::PH*^{PLC}) (ref. 32), *mat-1(ax227)* (ref. 7), *spd-5(or213)* (ref. 8), *ect-2(ax751)* (ref. 4), *par-1(it51); rol-4(sc8)/DnT1* (ref. 14), *par-1(b274); rol-4(sc8)/DnT1* (ref. 14), *par-3(it71);unc-32(e189)/qC1* (ref. 33) and *par-2(ok1723)/sC1(dpy-1(s2170))* from *C. elegans* Gene Knockout Consortium. Strains were maintained at 20 °C, except for *mat-1(ax227)* and *spd-5(or213)* maintained at 16 °C. All strains were shifted to 25 °C for 20–30 h before recording.

RNAi. RNAi was carried out by feeding[34] (*par-1*) or soaking[35] (all other genes). Primers for RNA production are listed in Supplementary Table S4.

Microscopy. For live-cell imaging, embryos in egg salt buffer were placed onto coverslips and inverted on 2–3% agarose pads on slides. For nocodazole treatment, embryos were permeabilized by gentle pressure on poly-L-lysine-coated slides with 10 mg ml^{-1} nocodazole in egg salt buffer[36]. Embryos were observed at 25 °C with a PlanApochromat ×63 1.4 NA oil-immersion lens on a Zeiss imager Z1 upright microscope (Carl Zeiss) outfitted with a CSUX-A1 spinning-disc confocal system (Yokogawa Electric) with LaserStack 491 and 561 solid-state diode lasers (Intelligent Imaging Innovation). Images were acquired with a Cascade QuantEM 512 SC camera (Photometrics) controlled by Slidebook software (Intelligent Imaging Innovations) every 5 s using 400 ms exposure for GFP::PAR-2 and 600 ms for mCherry::tubulin at 100% power on the lasers and 1×1 binning in the camera. Nuclear envelope breakdown was defined as the first time frame when the GFP fusion was no longer excluded from pronuclei.

For immunofluorescence microscopy, embryos were fixed on poly-L-lysine-coated slides in −20 °C methanol for 20 min and −20 °C acetone for 10 min, and stained with rabbit 1:100 anti-PAR-2 (ref. 37), 1:100 rabbit anti-PAR-1 (ref. 14), 1:300 rabbit anti-GFP (Invitrogen), 1:60 mouse anti-PAR-3 (P4A1; ref. 38), 1:1,000 mouse anti-tubulin (DM1A; Sigma), 1:300 mouse anti-GFP (Roche) or 1:300 rat anti-PKC-3 (ref. 39). The secondary antibody was 1:1,000 goat anti-rabbit coupled to Alexa488, 1:1,000 goat anti-rabbit coupled to Cy3, 1:1,000 goat anti-mouse coupled to Cy3 or 1:1,000 goat anti-rat coupled to Cy2 (Molecular Probes). For co-staining of mCherry::PH^{PLC} and GFP::PAR-2, zygotes were fixed in methanol for 10 s and 2% formaldehyde in PBS for 30 min, and stained with 1:300 rabbit anti-dsRed (Clontech) and 1:300 mouse anti-GFP (Roche). Slides were counterstained with DAPI and imaged as above.

Protein preparation. GST fusions were cloned in pGEX6p-1 (GE Healthcare), prepared according to the manufacturer's protocol (GE Healthcare) and exchanged into H100 buffer (50 mM HEPES at pH 7.4, 1 mM EGTA, 1 mM $MgCl_2$, 100 mM NaCl, 10% glycerol and 0.05% NP-40). GST::PAR-1::FLAG fusion was further purified with EZview red M2 beads (Sigma), and exchanged into H100 buffer. GST was cleaved off by incubation with PreScission protease, and exchanged into binding buffer (80 mM PIPES at pH 6.8, 1 mM EGTA, 1 mM $MgCl_2$ and 40 mM NaCl) for co-sedimentation assay and kinase assay or into H100 buffer for GST pulldown assay. Protein concentrations were determined using the Bradford protein assay relative to a BSA standard. Purified PAR-2 was pre-cleared at 98,000*g* for 20 min in a TLA55 rotor (Bechman Coulter).

MBP fusions were cloned in pMALc2x (New England Biolabs) and prepared according to the manufacturer's protocol.

Microtubule-binding assay. Microtubules were assembled from tubulin (bovine brain, Cytoskeleton) in the presence of 1 mM GTP for 20 min at 37 °C and stabilized with 20 μM taxol. Dilutions were made in binding buffer (80 mM PIPES at pH 6.8, 1 mM EGTA, 1 mM $MgCl_2$ and 40 mM NaCl) supplemented with 20 μM taxol. Varying concentrations (0.06–6 μM) of polymerized tubulin were incubated with recombinant PAR-2 (0.25 μM or 2.5 nM) at room temperature for 30 min. The PAR-2/microtubule mixture was pelleted over 100 μl of binding buffer with 40% glycerol at 98,000*g* for 20 min in a TLA55 rotor. For the assay with 0.25 μM PAR-2, equivalent amounts of supernatant and pellet were run on a 4–12% SDS polyacrylamide gel (Invitrogen) and stained with Coomassie. For the assay with 2.5 nM PAR-2, equivalent amounts of input and pellet were run on a gel as above, blotted onto Hybond LFP membranes (GE Healthcare) and detected with rabbit 1:500 anti-PAR-2 antibody[37] and 1:2,000 goat anti-rabbit coupled to Cy5 by a fluorescent laser scanner Typhoon 9410 (GE Healthcare). The percentage of pelleted PAR-2 relative to the input was determined in the same gel by densitometry using ImageJ software. The dissociation constant (K_d) was determined with Prizm 4 (GraphPad).

To visualize recombinant PAR-2 on microtubules, 3.3 mg ml^{-1} tubulin and 1.7 mg ml^{-1} rhodamine-labelled tubulin from bovine brain (Cytoskeleton) were polymerized to microtubules by incubation with 1 mM GTP for 20 min at 37 °C and stabilized by 20 μM taxol. Microtubules and purified GFP::PAR-2 were incubated for 10 min at room temperature. Images were acquired by epifluorescence microscopy with a PlanApochromat ×63 1.4 NA oil-immersion lens on a Zeiss imager Z1 upright microscope (Carl Zeiss).

Kinase assays. For PAR-2, 1.0 μM PAR-2 was incubated for 20 min at room temperature with or without 20 μM taxol-stabilized microtubules or with microtubules that had been depolymerized with 10 μM nocodazole. Samples were mixed with 29 fM recombinant human PKC (Millipore) in kinase buffer (20 mM HEPES at pH 7.4, 5 mM $MgCl_2$ and 1 mM dithiothreitol) containing 60 μM cold ATP and 2.3 μCi [γ-^{32}P]ATP at room temperature, and kinase reactions were carried out by incubating samples at 30 °C or on ice (for time 0 samples) and terminated by adding 4× Laemmli SDS sample buffer. Proteins were separated by a 7% Tris-acetate gel (Invitrogen) and stained with Coomassie, and phosphorylation was visualized by autoradiography. Wild-type PAR-2 without microtubules was included in every experiment and used as a standard to measure the relative amount of phosphorylation. ATP incorporation was determined by measuring the amount of incorporated and unincorporated [γ-^{32}P]ATP in autoradiograph images of 4–12% SDS polyacrylamide gel (Invitrogen) frozen at −20 °C. Michaelis–Menten kinetic curves were generated with Prizm 4 (GraphPad).

For PAR-3/1, PAR-3 fusions and MBP::PAR-1(753–1192 aa) were incubated with MBP::PAR-1(1–492 aa with T325E mutation) or 0.2 U recombinant human aPKC (Calbiochem) at 30 °C for 30 min or 37 °C for 30 min, respectively. Kinase reactions were terminated by adding 4× Laemmli SDS sample buffer.

GST pulldown assay. GST fusions were incubated with PAR-2, PAR-1(1–964)::FLAG or PAR-1(965–1192)::FLAG at 4 °C for 1 h, incubated with glutathione agarose (GE Healthcare) at 4 °C for 30 min and washed with H100 buffer. Equivalent amounts of supernatant and pellet were run on a 4–12% SDS polyacrylamide gel (Invitrogen) and stained with Coomassie.

Immunoblotting of extracts from *C. elegans* gravid adults. Extracts from gravid adults were prepared as previously described[12]. GFP fusions and tubulin were visualized using 1:1,000 mouse anti-GFP antibody (Roche) and 1:2,000 anti-tubulin antibody (DM1A; Sigma), respectively. Horseradish peroxidase (HRP)-conjugated anti-mouse antibody (GE Healthcare) was used as a secondary antibody and detected with chemiluminescence microscopy.

Immunoprecipitation of GFP fusions from worm extracts. *C. elegans* embryos of mixed stages were collected from gravid adults by a standard method and suspended in an equal volume of H100 buffer with protease inhibitor (Roche). The embryo suspension was frozen in liquid nitrogen, ground with a mortar and pestle and centrifuged at 4 °C, 20,800*g* for 50 min. A volume of 500 μl of extracts from wild-type embryos expressing GFP, *par-2(ok1723)* embryos expressing GFP::PAR-2 and wild-type embryos expressing GFP::PAR-1$^{965\text{–}1192}$ and 3 ml of extract from *par-1(b274)* expressing GFP::PAR-1 was incubated with 20 μl of GFP-Trap beads (Allele Biotechnology). After an overnight incubation, the beads were washed with H100 buffer and resuspended with 50 μl of 1× Laemmli SDS sample buffer, and heated at 90 °C for 5 min. GFP fusions, PAR-2 and PAR-1 were visualized using 1:1,000 mouse anti-GFP (Roche), 1:2,000 rabbit anti-PAR-2 (ref. 24) and 1:300 rabbit anti-PAR-1 (ref. 14). HRP-conjugated anti-mouse antibody (GE Healthcare) was used as a secondary antibody and detected with chemiluminescence microscopy.

FRAP. A square with 8 μm sides on the cortex of *pkc-3(RNAi)* zygotes (1 min post-pronuclear meeting) was photobleached using a MicroPoint Mosaic (Photonic Instruments) at full power for 2 s. GFP::PAR-2 images were captured using the 491 solid-state diode laser line at full power with an exposure time of 500 ms. Fluorescence recovery half-time ($t_{1/2}$) was measured for a 2.5 μm square at the boundary (Out) and at the centre (In) of the bleached region by the FRAP analyser module function in Slidebook software (Intelligent Imaging Innovations), which fits an exponential decay curve to the data.

Protein–lipid binding assay. Recombinant GST::PAR-2 (2 μg) was incubated for 15 min at room temperature with or without 1.5 μM polymerized tubulin stabilized with taxol. Samples were mixed with 50 fM recombinant human PKC (Millipore) in kinase buffer containing 60 μM ATP, and kinase reactions were carried out by incubating samples at 30 °C for 20 min. Samples were then incubated at room temperature for 30 min with lipid strips (Echelon) pre-blocked with kinase buffer containing 3% fatty-acid-free BSA (Sigma) and washed with TBS containing 0.1 % (v/v) Nonidet-P40. The GST fusions were visualized using 1:5,000 rabbit polyclonal anti-GST antibody coupled to HRP (Santa Cruz Biotechnology). GST::PAR-2 alone was used as a standard in every experiment.

Statistical analysis. Statistical significance was measured by a two-tailed Student's *t*-test.

30. Kachur, T., Audhya, A. & Pilgrim, D. UNC-45 is required for NMY-2 contractile function in early embryonic polarity establishment and germline cellularization in *C. elegans*. *Dev. Biol.* **314,** 287–299 (2008).
31. Etemad-Moghadam, B., Guo, S. & Kemphues, K. Asymmetrically distributed PAR-3 protein contributes to cell polarity and spindle alignment in early *C. elegans* embryos. *Cell* **83,** 743–752 (1995).
32. Merritt, C. & Seydoux, G. Transgenic solutions for the germline. *WormBook* 1–21 (2010).
33. Praitis, V., Casey, E., Collar, D. & Austin, J. Creation of low-copy integrated transgenic lines in *Caenorhabditis elegans*. *Genetics* **157,** 1217–1226 (2001).
34. Maeda, I., Kohara, Y., Yamamoto, M. & Sugimoto, A. Large-scale analysis of gene function in *Caenorhabditis elegans* by high-throughput RNAi. *Curr. Biol.* **11,** 171–176 (2001).
35. Kamath, R. *et al*. Systematic functional analysis of the *Caenorhabditis elegans* genome using RNAi. *Nature* **421,** 231–237 (2003).
36. Hannak, E., Kirkham, M., Hyman, A. A. & Oegema, K. Aurora-A kinase is required for centrosome maturation in *Caenorhabditis elegans*. *J. Cell Biol.* **155,** 1109–1116 (2001).
37. Dong, Y., Bogdanova, A., Habermann, B., Zachariae, W. & Ahringer, J. Identification of the *C. elegans* anaphase promoting complex subunit Cdc26 by phenotypic profiling and functional rescue in yeast. *BMC Dev. Biol.* **7,** 19 (2007).
38. Nance, J., Munro, E. & Priess, J. *C. elegans* PAR-3 and PAR-6 are required for apicobasal asymmetries associated with cell adhesion and gastrulation. *Development* **130,** 5339–5350 (2003).
39. Aono, S., Legouis, R., Hoose, W. & Kemphues, K. PAR-3 is required for epithelial cell polarity in the distal spermatheca of *C. elegans*. *Development* **131,** 2865–2874 (2004).

nature cell biology

DOI: 10.1038/ncb2354

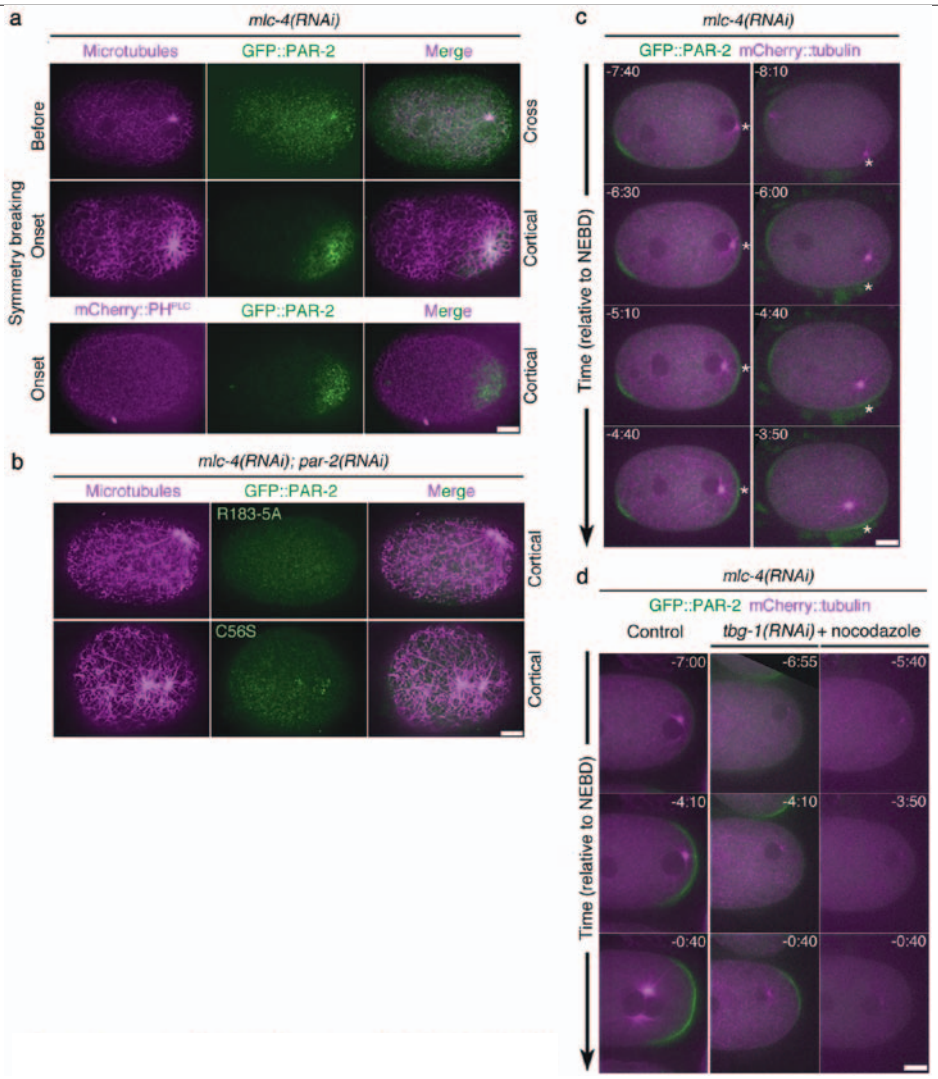

Figure S1 GFP::PAR-2 localization during symmetry breaking. (**a**) Confocal images of fixed *mlc-4(RNAi)* zygotes expressing GFP::PAR-2 fusions and mCherry::PH^{PLC}, a plasma membrane marker, stained for tubulin or mCherry::PH^{PLC} (magenta) and GFP (green). Cross-sections and cortical sections are shown. Note that GFP::PAR-2 and mCherry::PH^{PLC} do not show the same pattern at the site of MTOC/cortex contact, indicating that the PAR-2 cortical pattern is not simply caused by plasma membrane deformation. Scale bar, 10 μm. (**b**) Confocal images of fixed *mlc-4(RNAi);par-2(RNAi)* zygotes expressing GFP::PAR-2 fusions stained for tubulin (magenta) and GFP (green). Cortical sections are shown. Whereas wild-type GFP::PAR-2 is highest at the MTOC (25 of 30), GFP::PAR-2(R183-5A) does not associate with the MTOC or cortex (0 of 26), and GFP::PAR-2(C56S) associates with the MTOC (14 of 25) but does not spread on the cortex away from the MTOC. Scale bar, 10 μm. (**c**) Fluorescence micrographs from two time-lapse movies of *mlc-4(RNAi)* zygotes expressing GFP::PAR-2 (green) and mCherry::tubulin (magenta). The position (asterisk) of the MTOC along the cortex at symmetry breaking was determined in the first frame, and matches the center of the cortical PAR-2 domains that become visible in the later time points. In the movies, the GFP::PAR-2 domain rises above background only after the MTOC returns in the cytoplasm because of the lower sensitivity of live imaging, but in fixed zygotes the domain is already visible when the MTOC is against the cortex (Supplementary Fig. S1a). The GFP::PAR-2 patch that forms on the anterior cortex is caused by the meiotic spindle remnant, which can also promote GFP::PAR-2 cortical localization[18]. Scale bar, 10 μm. (**d**) Symmetry breaking by PAR-2 requires microtubules. Time-lapse images of GFP::PAR-2 and mCherry::tubulin in posterior region of *mlc-4(RNAi)* zygotes treated with DMSO (control) or nocodazole and γ-*tubulin/tbg-1(RNAi)*. As in Supplementary Fig. S1c, GFP::PAR-2 becomes visible on the cortex several minutes after the MTOC has returned in the cytoplasm due to limited sensitivity of live imaging. Note that nocodazole and *tbg-1(RNAi)* treatment does not eliminate all microtubules at the MTOC. Treated zygotes fell into two classes: one class that formed GFP::PAR-2 domains that appeared later and were smaller than wild type (first experimental column) and a second class that never localized GFP::PAR-2 to the cortex (second experimental column). NEBD is nuclear envelope breakdown (first mitosis). Scale bar, 10 μm.

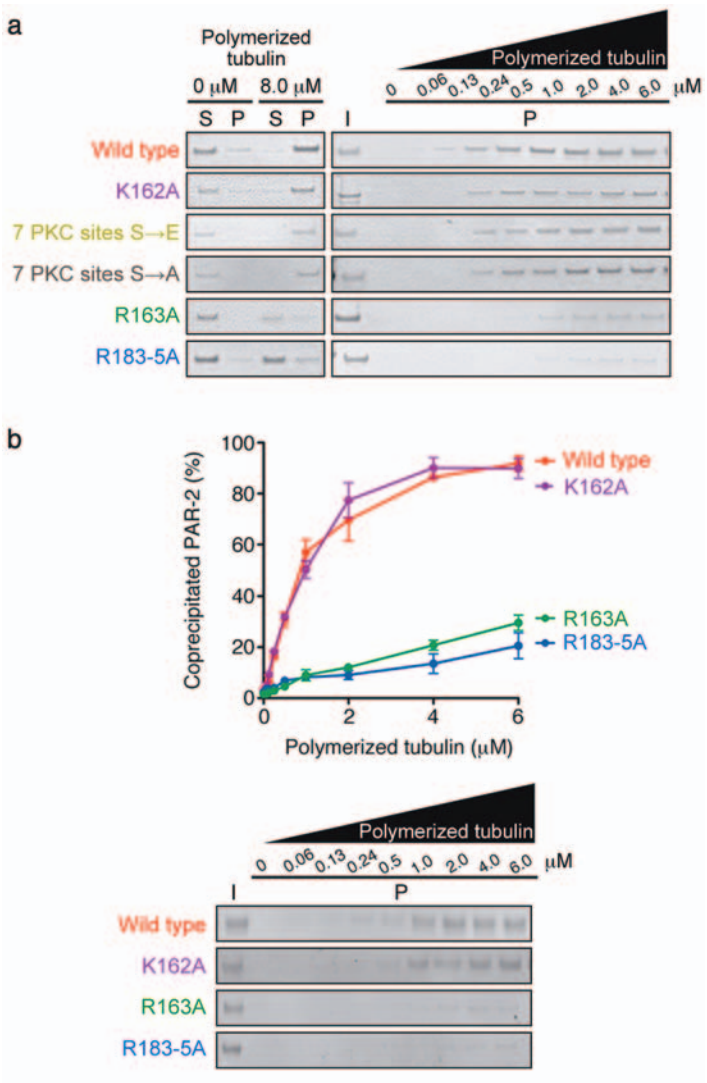

Figure S2 PAR-2 has microtubule-binding activity. (**a**) *In vitro* cosedimentation of wild-type and mutant PAR-2 with microtubules. PAR-2 in the input (I), the supernatant (S) and the pellet (P) fractions at the indicated concentrations of polymerized tubulin were monitored by Coomassie staining. (**b**) Same as Fig. 2b and Supplementary Fig. S2a except that 2.5 nM PAR-2 was used to maintain tubulin in excess. PAR-2 in the input (I) and the pellet (P) fractions were monitored by quantitative immunoblotting. Using wild-type PAR-2, we derived from this graph a Kd of 1.19 μM, which is significantly higher than that of Tau (Kd=0.16 μM; Goode, B. and Feinstein, S. 1994 *J Cell Biol* **124**, 769-782).

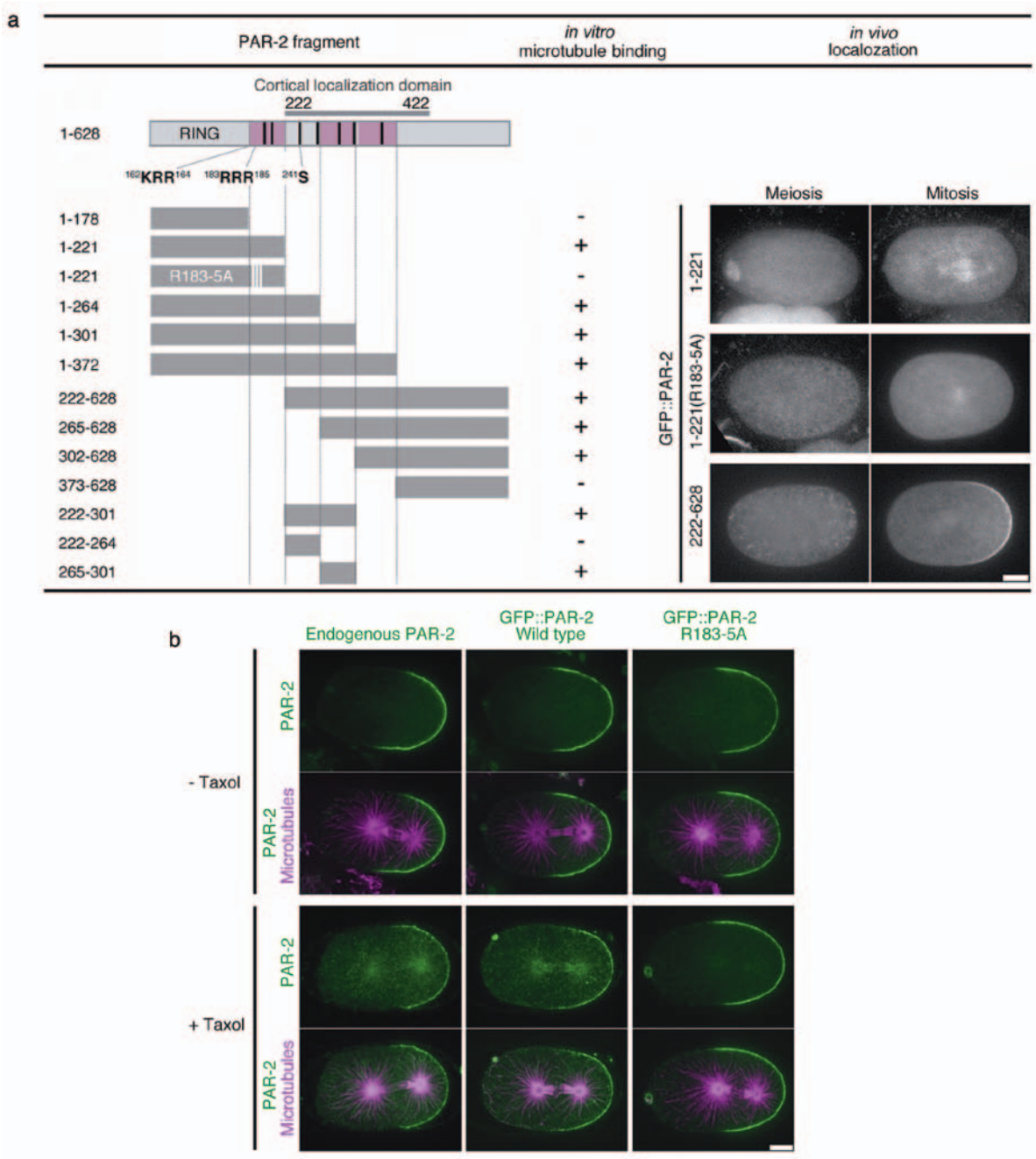

Figure S3 PAR-2 contains at least three microtubule-binding domains. (**a**) Summary from *in vitro* co-sedimentation assay with indicated PAR-2 fragments. Three PAR-2 domains are sufficient to bind microtubules: 1-221 aa, 265-301 aa, and 302-628 aa. Pink boxes highlights regions necessary (179-221 aa and 302-372 aa) or sufficient (265-301 aa) for binding within each domain. GFP::PAR-2(1-221) accumulated on spindles during meiosis and mitosis, but GFP::PAR-2(1-221(R183-5A)) did not. GFP::PAR-2(222-628) which includes the PAR-2 cortical localization domain was predominantly at the posterior cortex. Scale bar, 10 μm. (**b**) PAR-2 colocalizes with microtubules in zygotes treated with taxol. Confocal images of fixed zygotes stained for PAR-2 and tubulin, or fixed zygotes expressing GFP::PAR-2 or GFP::PAR-2(183-5A) stained for GFP and tubulin. Note that endogenous PAR-2 and GFP::PAR-2, but not GFP::PAR-2(R183-5A), localize to mitotic microtubules upon treatment with 40 μM taxol. Scale bar, 10 μm.

Figure S4 Alignment of PAR-2 domains comparing *C. elegans*, *C. briggsae*, and *C. remanei* PAR-2. *C. elegans* PAR-2 has three regions sufficient for microtubule binding (1-221 aa, 265-301 aa, and 302-628 aa: magenta box) and a region sufficient for cortical localization *in vivo* (222-428 aa: grey box). Magenta-striped box shows the region necessary for binding within each region (179-221 aa, 265-301 aa, and 302-372 aa). Basic residues critical for microtubule binding (^{163}R and ^{183}RRR^{185}) are indicated in magenta. A residue required for maximal phosphorylation by aPKC *in vitro* (^{241}S) is shown in green. Asterisk indicates positions of fully conserved residue. Colons and periods indicate conservation between groups of strong similarity (scoring > 0.5 in the Gonnet PAM 250 matrix) and weak similarity (scoring =< 0.5), respectively.

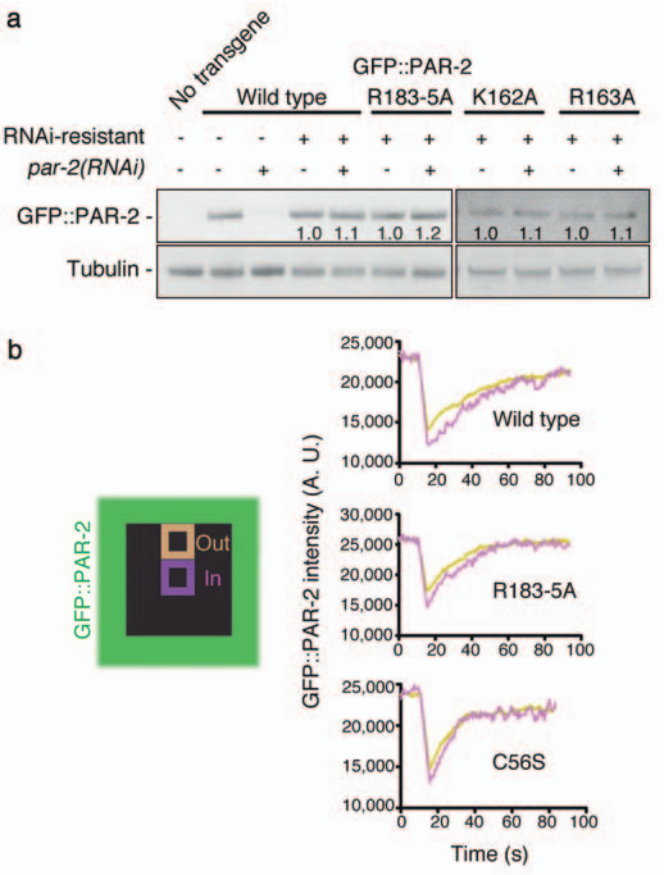

Figure S5 Analysis of cortical dynamics of GFP::PAR-2 fusions. (**a**) Immunoblotting analysis of GFP::PAR-2 fusions after RNAi against endogenous *par-2*. Extracts were prepared from worms expressing the indicated fusions and treated or not treated with RNAi. Extracts were immunoblotted with anti-GFP antibody and anti-tubulin antibody. RNAi-resistant fusions are expressed at similar levels and are not depleted after RNAi against endogenous PAR-2. Numbers indicate levels of GFP::PAR-2(R183-5A) and GFP::PAR-2(R163A) relative to wild-type GFP::PAR-2 and GFP::PAR-2(K162A), respectively, and normalized to tubulin levels. As determined by western blotting with anti-PAR-2 antibody, GFP::PAR-2 is expressed at 1.3-fold the level of endogenous PAR-2 (data not shown). (**b**) Fluorescence Recovery After Photobleaching (FRAP) analysis of GFP::PAR-2 dynamics at the cortex. FRAP was performed on the cortex of *pkc-3(RNAi)* zygotes expressing the indicated GFP::PAR-2 fusions as in reference[26]. Representative fluorescence recovery curves are shown. GFP::PAR-2(R183-5A) recovery is identical to wild-type GFP::PAR-2. GFP::PAR-2(C56S) recovers twice as fast compared to wild-type GFP::PAR-2. Fluorescence recovery at the center (In) was slower than that at the boundary (Out), indicating that GFP::PAR-2 was entering the bleached region at least in part through lateral diffusion, consistent with reference[26].

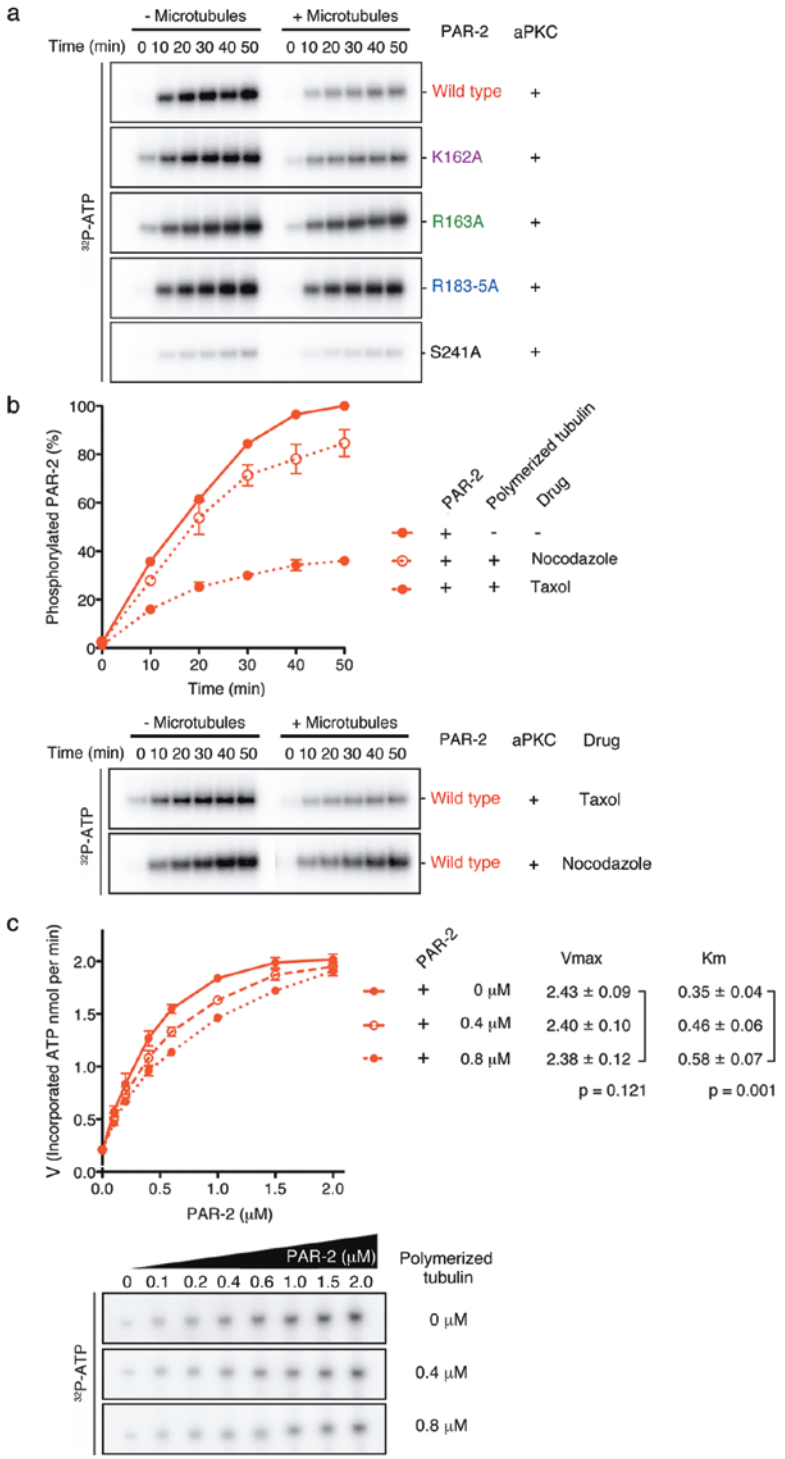

Figure S6 Microtubules protect PAR-2 from phosphorylation by aPKC. (**a**) PAR-2 was incubated with aPKC in the presence (right) or absence (left) of microtubules: PAR-2 wild-type and K162A bind microtubules, R163A and R183-5A do not. PAR-2 phosphorylation was monitored by ^{32}P-ATP incorporation. (**b**) PAR-2 was incubated with polymerized tubulin treated with nocodazole or taxol and added to the aPKC kinase reaction. The amount of phosphorylated PAR-2 relative to the condition without tubulin was measured by ^{32}P-ATP incorporation. Graph depicts the average percent of phosphorylated PAR-2 from three independent experiments. Error bars represent standard deviation. Times are with respect to the start of incubation at 30 ℃ after addition of aPKC. (**c**) Effect of microtubules on aPKC enzyme kinetics against PAR-2. Increasing concentrations of PAR-2 were incubated with 0, 0.4, or 0.8 μM polymerized tubulin and then added to an aPKC kinase reaction. The rate of ATP incorporation to PAR-2 was calculated by measuring incorporated and unincorporated ^{32}P-ATP after a 15 min reaction. Graph depicts Michaelis-Menten plot showing the average percent speed of ATP incorporation per min from three independent experiments. Error bars represent standard deviation. Addition of microtubules increased the K_m without affecting the V_{max} of the kinase reaction, indicating that microtubules act as a competitive inhibitor that interferes with binding between PAR-2 and aPKC.

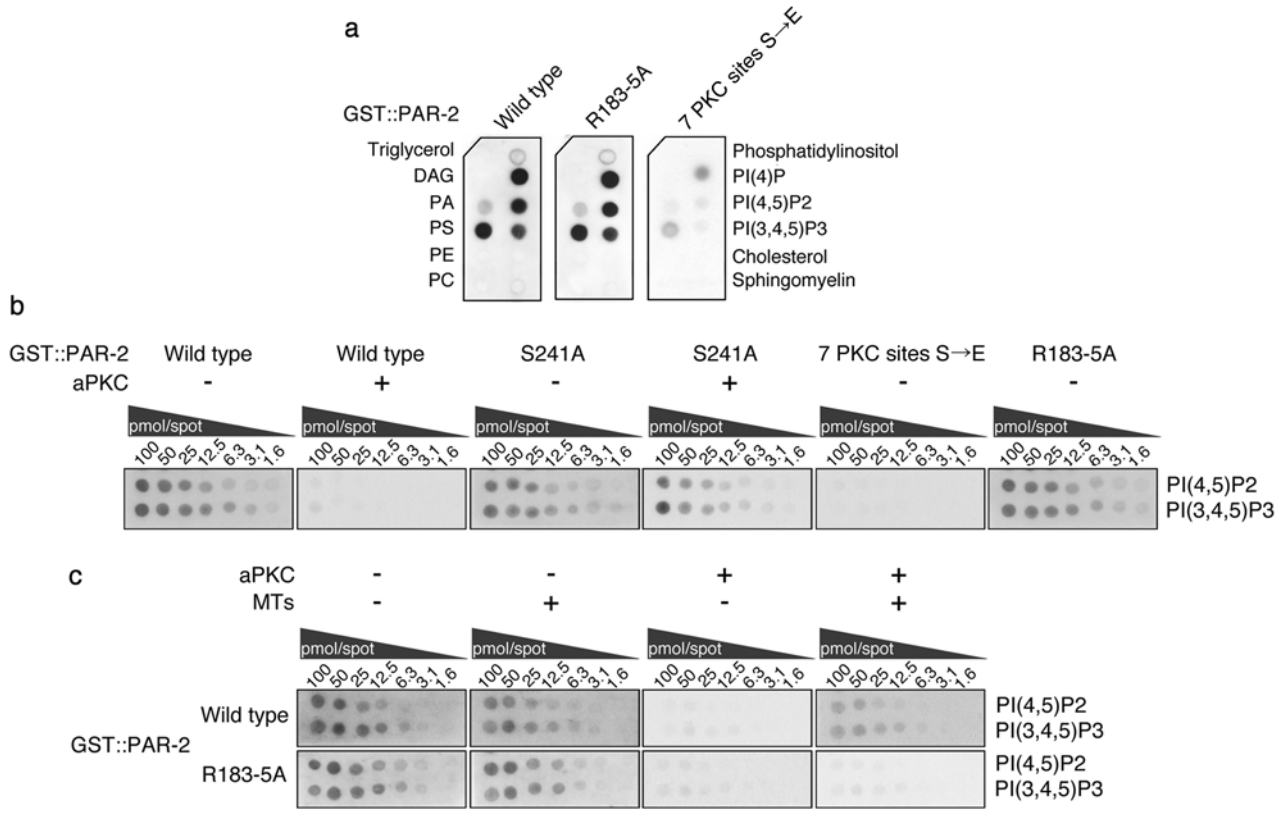

Figure S7 Binding to microtubules allows PAR-2 to interact with phospholipids in the presence of aPKC. (**a**) Protein-lipid binding assays with GST::PAR-2 fusions. Lipids spotted on the left and right columns are indicated. Wild-type PAR-2 and the microtubule-binding mutant R183-5A show identical lipid-binding specificities. The phoshomimetic mutant (7 PKC sites S→E) has reduced affinity. All blots were treated in parallel using identical conditions. (**b**) Phosphorylation by aPKC inhibits PAR-2 from binding to phospholipids. Protein-lipid binding assays with GST::PAR-2 fusions with or without aPKC phosphorylation. All blots were treated in parallel using identical conditions. (**c**) Binding to microtubules is sufficient to protect PAR-2 from aPKC and retain binding to phospholipids. Protein-lipid binding assays with GST::PAR-2 and aPKC with or without microtubules. Microtubules rescued lipid binding to wild-type PAR-2 but not PAR-2(R183-5A). All blots were treated in parallel using identical conditions.

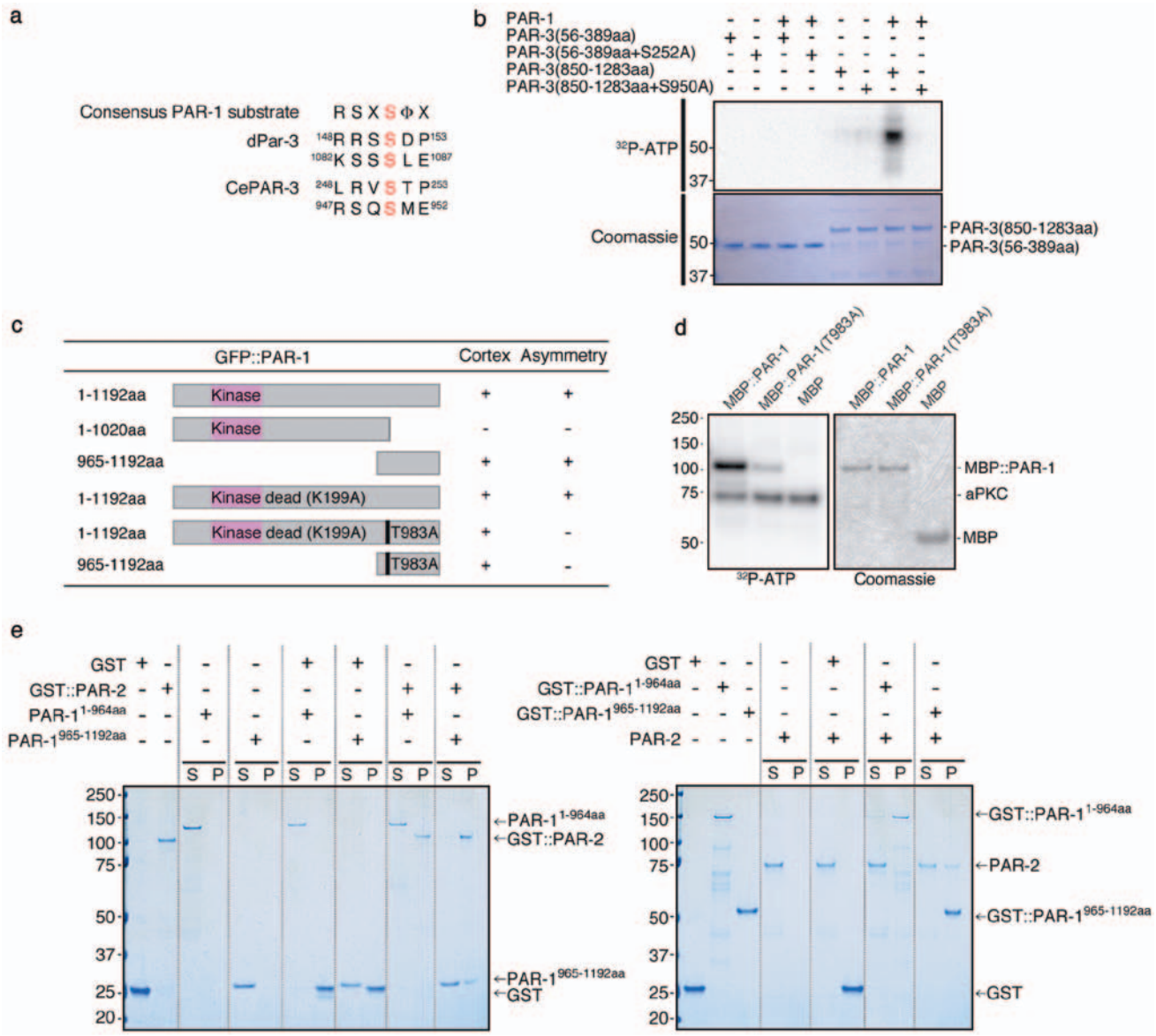

Figure S8 PAR-1 interacts with PAR-2 via its cortical localization domain and phosphorylates PAR-3. (**a**) Alignment of consensus PAR-1 phosphorylation sites (Nesić, D. *et al.* 2010 *Nat Struct Mol Biol* **17**, 130-132) in *Drosophila* dPAR-3 and *C. elegans* PAR-3. *Drosophila* PAR-1 phosphorylates both S151 and S1085[13]. (**b**) PAR-3 is a substrate for PAR-1 *in vitro*. Kinase assays using *C. elegans* MBP::PAR-1 and purified PAR-3 fusions. MBP::PAR-1 phosphorylates PAR-3(850-1283aa) but not PAR-3(850-1283aa + S950A) nor PAR-3(56-389aa), suggesting that S950 is the primary PAR-1 site in *C. elegans* PAR-3. (**c**) PAR-1 utilizes its C-terminal domain containing a PKC phosphorylation site for cortical localization. Schematics of GFP::PAR-1 fusions tested for localization *in vivo*. K199A is a mutation that inactivates the kinase activity of PAR-1 (used here to permit the generation of lines that mislocalize PAR-1) and T983A is a mutation in the conserved aPKC site. (**d**) PAR-1 is a substrate for aPKC *in vitro*. Kinase assays using aPKC and purified MBP::PAR-1(753-1192 aa) fusions or MBP. aPKC phosphorylates MBP::PAR-1 but not MBP::PAR-1(T983A) and MBP. Note that aPKC also autophosphorylates. (**e**) PAR-2 directly interacts with the PAR-1 C-terminus *in vitro*. *Left gel*: Purified GST and GST::PAR-2 were incubated with purified PAR-1$^{1\text{-}964}$ and PAR-1$^{965\text{-}1192}$, and the GST fusions were pulled down with glutathione agarose beads. *Right gel*: Purified GST, GST::PAR-1$^{1\text{-}964}$ and GST::PAR-1$^{965\text{-}1192}$ were mixed with purified PAR-2, and the GST fusions were pulled down with glutathione agarose beads. Proteins in the supernatant (S) and the pellet (P) fractions were monitored by Coomassie staining. GST::PAR-2 pulled down PAR-1$^{965\text{-}1192}$, but not PAR-1$^{1\text{-}964}$. Conversely, GST::PAR-1$^{965\text{-}1192}$, but not GST::PAR-1$^{1\text{-}964}$, pulled down PAR-2.